Proceedings of the ASME 2010 3rd Joint US-European Fluids Engineering Summer Meeting and 8th International Conference on Nanochannels, Microchannels, and Minichannels
FEDSM-ICNMM2010
August 1-5, 2010, Montreal, Canada

FEDSM-ICNMM2010-31237

A NOVEL DYNAMICS LATTICE BOLTZMANN METHOD FOR GAS FLOWS

C.T. Hsu
Mechanical Engineering Department, Hong Kong University of Science and Technology, Hong Kong
Email: mecthsu@ust.hk

S.W. Chiang
Mechanical Engineering Department, Hong Kong University of Science and Technology, Hong Kong
Email: mebench@ust.hk

K.F. Sin
Mechanical Engineering Department, Hong Kong University of Science and Technology, Hong Kong
Email: meskf@ust.hk

ABSTRACT

The lattice Boltzmann method (LBM), where discrete velocities are specifically assigned to ensure that a particle leaves one lattice node always resides on another lattice node, has been developed for decades as a powerful numerical tool to solve the Boltzmann equation for gas flows. The efficient implementation of LBM requires that the discrete velocities be isotropic and that the lattice nodes be homogeneous. These requirements restrict the applications of the currently-used LBM schemes to incompressible and isothermal flows. Such restrictions defy the original physics of Boltzmann equation. Much effort has been devoted in the past decades to remove these restrictions, but of less success.

In this paper, a novel dynamic lattice Boltzmann method (DLBM) that is free of the incompressible and isothermal restrictions is proposed and developed to simulate gas flows. This is achieved through a coordinate transformation featured with Galilean translation and thermal normalization. The transformation renders the normalized Maxwell equilibrium distribution with directional isotropy and spatial homogeneity for the accurate and efficient implementation of the Gaussian-Hermite quadrature. The transformed Boltzmann equation contains additional terms due to local convection and acceleration. The velocity quadrature points in the new coordinate system are fixed while the correspondent points in the physical space change from time to time and from position to position. By this dynamic quadrature nature in the physical space, we term this new scheme as the dynamic quadrature scheme. The lattice Boltzmann method (LBM) with the dynamic quadrature scheme is named as the dynamic lattice Boltzmann method (DLBM). The transformed Boltzmann equation is then solved in the new coordinate system based on the fixed quadrature points.

Validations of the DLBM have been carried with several benchmark problems. Cavity flows problem are used. Excellent agreements are obtained as compared with those obtained from the conventional schemes. Up to date, the DLBM algorithm can run up to Mach number at 0.3 without suffering from numerical instability. The application of the DLBM to the Rayleigh-Bernard thermal instability problem is illustrated, where the onset of 2D vortex rolls and 3D hexagonal cells are well-predicted and are in excellent agreement with the theory.

In summary, a novel dynamic lattice Boltzmann method (DLBM) has been proposed with algorithm developed for numerical simulation of gas flows. This new DLBM has been demonstrated to have removed the incompressible and isothermal restrictions encountered by the traditional LBM.

INTRODUCTION

The lattice Boltzmann method (LBM) is pioneered by several researchers, particularly McNamara and Zanetti [1], and can be viewed as a simplified finite difference solver of the Boltzmann equation on a discrete lattice [2, 3]. The lattice Boltzmann equation, i.e. a lattice analogy of the Boltzmann equation, provides an alternative description of the evolution of particle distribution that can be solved efficiently with an LBM algorithm. With the simplicity of algorithm that has retained

most physical properties but little statistical noise, the LBM was used widely and indistinguishably to study many classical fluid problems, including turbulence, single and multiphase flows, porous flows, colloidal flows, etc. Its use in multi-scale problems has also attracted much recent interests in the method [4]. It is also a favourable platform for designing algorithm to tackle multi-physics problems. Some examples include multiphase flows, particulate flows, micro-flows and transitional *Kn* regime flows [4], and acoustic propagations [5].

The LBM has been understood as a self-contained special discrete finite difference form of the original Boltzmann equation [6, 7], and is considered as a specific case of the discrete ordinate method (DOM) mathematically [8]. It is a lattice technique for the solution of the Boltzmann equation, and is found to be effective for solving incompressible flows. The performance of the LBM has been compared with the conventional CFD methods, to demonstrate that LBM is a robust and accurate numerical method for solving NSF equations of very low Mach number flows [2, 9].

Nevertheless, the LBM has its limitation in solving the Boltzmann equation. Essentially, the implementation of LBM requires that the discrete velocities be *isotropic* and that the lattice nodes be *homogeneous*. These requirements restrict the conventional LBM schemes only applicable to incompressible and isothermal flows. In the past decades, much efforts have been devoted to the development of thermally enabled LBM [10]. Different kinds of thermal LBM have been proposed in decades, but they are of less satisfactory due to various deficiencies, such as non-Galilean invariance and instabilities inherited in the thermal scheme [11]. These existing workarounds have not been directed to the above essential requirements. The resulting restrictions, such as isothermal and very low Mach number, defy the original physics of Boltzmann equation. Much effort has been devoted in the past decades to remove these restrictions, but of less success.

In this paper, a novel dynamic lattice Boltzmann method (DLBM) that is free of the incompressible and isothermal restrictions is proposed and developed to simulate gas flows. This is achieved through a coordinate transformation featured with Galilean translation and thermal normalization. The transformation renders the normalized Maxwell equilibrium distribution with directional isotropy and spatial homogeneity for the accurate and efficient implementation of the Gaussian-Hermite quadrature. The velocity quadrature points in the new coordinate system are fixed while the correspondent points in the physical space change from time to time and from position to position. By this dynamic quadrature nature in the physical space, we term this new scheme as the dynamic quadrature scheme. The lattice Boltzmann method (LBM) with the dynamic quadrature scheme is named as the dynamic lattice Boltzmann method (DLBM).

In this paper, the transformed Boltzmann equation was solved for the viscous cavity flows and the Rayleigh-Benard instability, with BGK collision model (DLBM-BGK) [12, 13]. Excellent agreements with the results obtained from the conventional macroscopic NSF equations were achieved.

DYNAMIC DISCRETE ORDINATE METHOD

The Boltzmann equation, derived from statistical mechanics based on gas kinetic theory, describes the evolution of the velocity distribution function $f(\mathbf{r},\mathbf{c},t)$ of dilute gases of identical molecules in the phase space and with the BGK collision model is given by

$$\frac{\partial f}{\partial t}+\mathbf{c}\cdot\frac{\partial f}{\partial \mathbf{r}}+\mathbf{F}\cdot\frac{\partial f}{\partial \mathbf{c}}=\Omega=-\frac{1}{\tau}(f-f^{eq}) \tag{1}$$

where τ is the molecular collision relaxation time. The equilibrium velocity distribution $f^{eq}(\mathbf{r},\mathbf{c},t)$ is given by the Maxwell distribution,

$$f^{eq}(\mathbf{r},\mathbf{c},t)=n(\frac{m}{2\pi kT})^{\frac{3}{2}}\exp(-\frac{m(\mathbf{c}-\mathbf{u})^2}{2kT})\cdot \tag{2}$$

In (2), $\rho(\mathbf{r},t)$, $\mathbf{u}(\mathbf{r},t)$ and $T(\mathbf{r},t)$ are the macroscopic density, mean velocity and temperature of the gas, which can be obtained by taking the first three moments of the distribution function:

$$\begin{aligned}\int f d^3c &= \int f^{eq} d^3c = n\\ \int \mathbf{c} f d^3c &= \int \mathbf{c} f^{eq} d^3c = n\mathbf{u}\\ \tfrac{1}{2}\int \mathbf{c}^2 f d^3c &= \tfrac{1}{2}\int \mathbf{c}^2 f^{eq} d^3c = \tfrac{1}{2}nu^2 + ne\end{aligned} \tag{3a,b,c}$$

It is noted that the last equalities in (3) are satisfied by f^{eq} automatically by definition. They become the constraints to the efficiency in the discrete evaluation of the integrals (3).

To simplify the solution to (1)-(3), a discrete ordinate method (DOM) is used to approximate the integrals in (3) by the summation of integrand over quadrature points with appropriate weightings. The main task of the DOM is to properly select the quadrature points and the weightings to

minimize the error. For the Maxwell equilibrium distribution, the Gaussian-Hermite quadrature has been commonly used. Traditionally, the DOM was applied directly to **c** in (2), which leads to error that depends greatly on the shape of the temperature *T* and mean velocity **u**. More quadrature points are needed when the temperature difference and the mean velocity are large. To circumvent this problem, the following transformation is used,

$$\mathbf{C}^* = \frac{\mathbf{c}-\mathbf{u}}{\sqrt{2RT}} \tag{4}$$

where $R = k/m$. Equation (4) basically represents the composition of Galilean translation and thermal normalization of **c**. In term of $\mathbf{C}^*$, (2) becomes

$$f^{eq}(\mathbf{r},\mathbf{c},t) = n(\frac{1}{2\pi RT})^{\frac{3}{2}} \exp(-\mathbf{C}^{*2}) \tag{5}$$

where the shape of the exponential is independent of *T* and **u**. The integrals (3) expressed in Gaussian-Hermite quadrature now become

$$\begin{aligned}
\frac{1}{n}\int f^{eq}(\mathbf{r},\mathbf{c},t)d^3c &= (\pi)^{-3/2}\int \exp(-C^{*2})d^3C^* \\
&= \sum_{i=1}^{N} w_i F_i = 1 \\
\frac{1}{n\sqrt{2RT}}\int (\mathbf{c}-\mathbf{u}) f^{eq}(\mathbf{r},\mathbf{c},t)d^3c &= (\pi)^{-3/2}\int \mathbf{C}^* \exp(-C^{*2})d^3C^* \\
&= \sum_{i=1}^{N} w_i \mathbf{C}_i^* F_i = 0 \\
\frac{1}{4nRT}\int (\mathbf{c}-\mathbf{u})^2 f^{eq}(\mathbf{r},\mathbf{c},t)d^3c &= \frac{1}{2}(\pi)^{-3/2}\int C^{*2} \exp(-C^{*2})d^3C^* \\
&= \frac{1}{2}\sum_{i=1}^{N} w_i C_i^{*2} F_i = \frac{3}{4}
\end{aligned} \tag{6a,b,c}$$

where $F_i = \pi^{-3/2}$. The quadrature points $\mathbf{C}_i^*$ and the weightings w_i can be determined mathematically from the Gaussian-Hermite polynomial of *N*-degree. In (6), a polynomial of $N \geq 2$ will result in *zero* error. The salient feature is that the quadrature points are fixed and independence of the mean velocity and temperature, i.e., independence of the Mach number of the gas flows. We noted that an expression similar to (4) had also been employed by Albright [14] and Smith [15] to replace the random sample procedure for reducing the high numerical noise in DSMC.

As from (4), the qaudrature points $\mathbf{c}_i$ will change with time and location in real space, this scheme was termed as the dynamic quadrature scheme. A discrete ordinate method with the dynamic quadrature scheme was then termed as the Dynamic Discrete Ordinate Method (DDOM) [12, 16].

DYNAMIC LATTICE BOLTZMANN METHOD

The LBM is a subset of DOM where the discrete velocities are specifically assigned to ensure that particle leaves one node will end at other nodes. In LBM, the fixed discrete velocity set is applied over the entire computation domain disregarding the orientation. Therefore it can only be applied efficiently for the isotropic and homogeneous distributions. In traditional LBM, $\mathbf{c}_i$ is used as the fixed discrete velocity set. This requires to expand f^{eq} in small Mach number and truncate at certain order due to the anisotropy of f^{eq} in $\mathbf{c}$. The truncation leads to errors which increase with Mach number. From the discussion in the last section, it appears that $\mathbf{C}_i^*$ will be better to use as the fixed discrete velocity set since no expansion and truncation will be required. To this end, we transformed the Boltzmann equation through the following coordinate transformation,

$$d\mathbf{r}^* = \frac{d\mathbf{r}}{a\tau_0}, \quad \mathbf{C}^* = \frac{\mathbf{c}-\mathbf{u}}{a}, \quad dt^* = \frac{dt}{\tau_0} \tag{7}$$

where τ_0 is a constant reference time and $a = \sqrt{2RT}$ is the sound speed. The Boltzmann equation in the new transformed coordinates $(\mathbf{r}^*, \mathbf{C}^*, t^*)$ now becomes

$$\begin{aligned}
&\frac{\partial f^*}{\partial t^*} + (\mathbf{C}^* + \mathbf{u}^*)\cdot\frac{\partial f^*}{\partial \mathbf{r}^*} + \mathbf{F}^*\cdot\frac{\partial f^*}{\partial \mathbf{C}^*} - \frac{\tau_0}{a}\frac{Da}{Dt}\mathbf{C}^*\cdot\frac{\partial f^*}{\partial \mathbf{C}^*} \\
&\quad - \frac{\tau_0}{a}\frac{D\mathbf{u}}{Dt}\cdot\frac{\partial f^*}{\partial \mathbf{C}^*} = \Omega^*
\end{aligned} \tag{8}$$

where $\frac{D}{Dt}=\frac{\partial}{\partial t}+\mathbf{c}\cdot\frac{\partial}{\partial \mathbf{r}}$ is a derivative evaluated in physical space, $f^*=\frac{f}{n_0}$, $\mathbf{u}^*=\mathbf{u}/a$, $\mathbf{F}^*=\frac{\mathbf{F}\tau_0}{a}$ and $\Omega^*=\frac{\Omega\tau_0}{n_0}$. Equation (8) shows that the transformation leads three additional terms associated with the convection due to $\mathbf{u}$ and the accelerations due to $\mathbf{u}$ and a. The constraints of the moments with respect to f^{eq} then become

$$\frac{1}{n^*}\int f^{*eq}d^3C^*=1$$
$$\frac{1}{n^*}\int \mathbf{C}^* f^{*eq}d^3C^*=0$$
$$\frac{1}{2n^*}\int C^{*2} f^{*eq}d^3C^*=\frac{3}{4} \qquad (9a,b,c)$$

which are equivalent to equation (6). Equations (8) and (9) can be solved with the LBM with the convection and acceleration terms treated as source terms. With the same reasons as DDOM, we name this new LBM using $\mathbf{C}_i^*$ as the fixed discrete velocity set as Dynamic Lattice Boltzmann Method (DLBM).

SIMPLIFIED DLBM FOR THERMAL FLOWS

The numerical procedure for the DLBM is a complicated procedure since it requires the Galilean translation in the **c** space and the local coordinate stretching in both the **c** and **r** spaces. For thermal problems where the temperature difference is not so large, it is possible to simplify the procedure by employing the Galilean translation only. This can be achieved by setting a as constant with $a=a_0=\sqrt{2RT_0}$ where T_0 is the reference temperature. Equation (8) is then reduced to

$$\frac{\partial f^*}{\partial t^*}+(\mathbf{C}^*+\mathbf{u}^*)\cdot\frac{\partial f^*}{\partial \mathbf{r}^*}+\mathbf{F}^*\cdot\frac{\partial f^*}{\partial \mathbf{C}^*}-\frac{D\mathbf{u}^*}{Dt^*}\cdot\frac{\partial f^*}{\partial \mathbf{C}^*}=\Omega^* \qquad (10)$$

This formulation is the same as the equation of change as in Chapman and Cowling [17] who focused on the mean velocity to establish the NS equations through the Chapman-Enskog expansion. Here we focus on the peculiar (thermal) velocity for employing the streaming process in the LBM procedure.

It is found that this simplified procedure is readily suitable for dealing with thermal LBM problems with moderate temperature change, and when the physical particle velocity is not altered for more than $0.3a_0$. Moreover, if higher temperature changes are encountered, one can always employ a larger discrete velocity set to improve the accuracy of capturing the variation due to high temperature differences, but this requires a different discrete velocity set and quadrature coefficients that will lose the optimality of the Gaussian-Hermite quadrature when the number of velocity is not 3 per dimension, i.e., D2Q9 for 2 dimensional flows or D3Q27 for a 3 dimensional system.

NUMERICAL PROCEDURE

In the implementation, we choose a D3Q27 lattice for the discretization of the phase space using Gaussian-Hermite quadrature coefficients. The streaming and collision procedures in the DLBM are similar to those of conventional LBM procedure. The acceleration term and convection term in equation (10) are discretized using central difference method. A Strange splitting algorithm is used to achieve 2nd order Lagrangian streaming. The boundary conditions on the wall are typical diffused reflection as in some conventional LBM. The details of the numerical procedure can be found in [18].

NUMERICAL RESULTS

Cavity Flows

The numerical domain is a square of size 100x100x5 to 500x500x5 with a dimensionless height H=2. The typical cavity velocity is U=0.2. The Reynolds number $Re=UH/\nu$ we employed in the simulations are 100, 400, and 1000. The DLBM is run until the average velocity magnitude has reached a steady state and changes less then 10^{-8} in magnitude. Different number of CPU cores is tried. The results shown in the following are for Re=100, 400, and 1000 with an OpenMP code running using an 8-cores dual-quad Dell Xeon workstation. As shown in Table 1, the vortex center positions are in agreement with the reference works within 1%. The small difference may arise from the current non-isothermal nature of the gas flows. These results show that the DLBM method can reproduce the main feature of the cavity flows.

Figure 1 shows the streamlines of the cavity gas flows as obtained from the present simulation for the cases of Re =100 and 1000. The flow patterns are in excellent agreements with those of the reference works [19, 20]. The evolution of internal energy e in the flow for the case of Re=1000 is shown in Figure 2, started from an initial internal energy value of e_0=0.55. All the walls were set to this initial temperature. We note that there is significant thermal evolution in the flow. This can constitute to extra stress in the flow and have considerable effects on the eventual steady flow pattern. The difference of the flow from ideal case will be more pronounced when there is gravitational

acceleration, to increases the difficulty for the comparison with experiment. In brief, the isothermal assumption commonly used in most cavity flow simulations may require reassessments.

Table 1 VORTEX CENTER POSITION :- COMPARISON OF THIS WORK WITH REFERENCES [19] [20].

Re	Primary vortex	Lower right vortex
100[19]	(0.6172,0.7390)	-
100 (this work)	(0.6220,0.7406)	-
400[20]	(0.5608,0.6078)	(0.8902,0.1255)
400 (this work)	(0.5621,0.6059)	(0.8880,0.1215)
1000[19]	(0.5333,0.5647)	(0.8667,0.1137)
1000 (this work)	(0.5459,0.5951)	(0.8688,0.1230)

Rayleigh-Benard Instability

The Rayleigh-Benard cell (RBC) patterns were produced from the numerical simulations based on full thermally driven Navier-Stokes equations with Boussinesq approximation [21-23]. Quasi-two-dimensional convective rolls are one simple form of convection in RBC over a range of lower Rayleigh numbers *Ra*, provided that the spatial distribution of the fluid does not exhibit significant vertical asymmetry with respect the the z=0 plane (Figure. 3). However, recent discovery that three-dimensional cellular flows are not prohibited in symmetric layers and, as established in recent years, can be stable within a certain region of the parameter space [24]. Such pattern has not been reproduced by numerical studies yet. It is known that RBC hexagons occur as the up-down symmetry of the velocity field is broken. One of the possible causes for such a symmetry breaking is the departure from Boussinesq approximation with probable significant change of fluid properties. When *Ra* is at the order of critical value Ra_c or higher, deviations from Boussinesq approximation can be quite significant [25]. Moreover, temperature difference gradually leads to extra stress in the fluid which drives the asymmetry further away. The patterns are estimated to be related to the variations of density, isobaric thermal expansion, kinematic viscosity, thermal conductivity, and specific heat with respect to the top and bottom temperatures. This may be a system too complex for correct macroscopic numerical modeling.

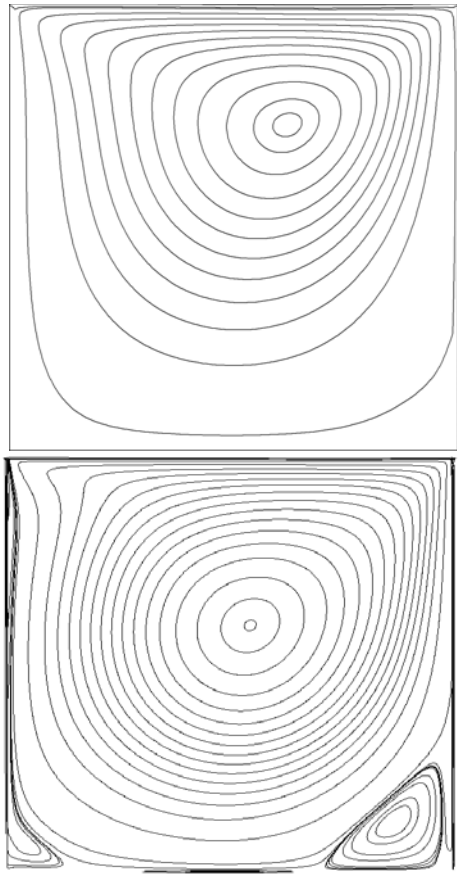

Figure 1. STREAMLINES OF THE LID DRIVEN CAVITY FLOWS WITH Re=100 and Re=1000.

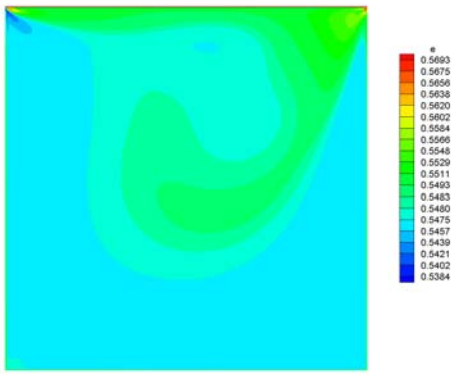

Figure 2. INTERNAL ENERGY DISTRIBUTION OF THE CASE Re=1000. THERE IS SIGNIFICANT INTERNAL ENERGY EVOLUTION IN THE CAVITY.

Flows of RBC describe a viscous fluid at rest between two horizontal parallel plates *z=0* and *z=d*, subjected to a typical

temperature difference ΔT with the lower plate at higher temperature. The direction of gravity is in the negative z-direction normal to the plates. Due to the local buoyant effect, the lower fluid with less density tends to move upwards, and the top heavier fluid tends to sink. The system becomes unstable when a dimensionless ΔT reaches a certain critical value. In particular, flows of RBC arise when Rayleigh number is sufficiently large. The critical Rayleigh number Ra_c depends on many physical parameters at different regime, including thermal expansivity α, gravitational acceleration g, separation distance between the two plates d, the typical temperature difference ΔT, kinematic viscosity ν, and thermal diffusivity κ. At the convective roll regime the significant convection phenomenon is the 2 dimensional rolls. Through non-linear stability analysis, the critical Rayleigh number Ra_C can be obtained to be about 1708 [26]. In the present simulations, our search for Ra_C starts from 1400 to 1900, with an increased interval of ΔRa_C =100, until the instability occurs. The critical wave number $a_C^* = \pi / W^* = \pi d / W$ was found to be around 3.12.

Figure 3 shows the simulation domain along with the coordinate system for the present numerical computation. The mesh size is different for each problem. Boundary conditions are set to simulate the asymmetric conditions at the top and bottom walls. The heated bottom is at a fixed temperature T_{bottom} and the cooled top plate is under a relaxation condition to the desired ambient temperature, corresponding to a constant overall heat flux losing to the environment from the top surface. The four vertical boundaries are two pairs of periodic boundaries which are paired consistently along each axis. The initial condition of the velocity in the entire domain is zero and the fluid temperature equals the cooled ambient temperature. For the 2-D convective roll case, both horizontal plates are of no-slip boundary. For the 3-D simulations, the cooled surface is a slip boundary and the heated surface is a no-slip wall. The Boussinesq approximation and the assumed fluid physical properties, which are usually used in macroscopic simulation, are not present in our computation.

A 2-D RBC is simulated using a domain with a very short dimension in the y-direction. The domain size is 137x7x23. The Δx employed for the DLBM is 0.02. A ΔT of 0.2 is established between the top and bottom plate. At the initial time t=0, the fluid in the domain is stagnant, and the **g** employed is 0.01 towards negative z direction. We searched for the instability through the range of Ra number as mentioned earlier and located its occurrence at 1600, and the corresponding flow fields, including the velocity vector **u** and its magnitude |**u**|, as well as the distributions of number density and energy (temperature), are shown in Figure 4 in color contour. Below this Ra number no instability is observed. When Ra =1600, the wave number obtained is approximately 3.12, which is close to the theoretical value given in [26] as predicted for flows under the incompressible assumption. We consider that our current result for weakly compressible flows represents the real fluids and is in a good agreement with the theoretical prediction.

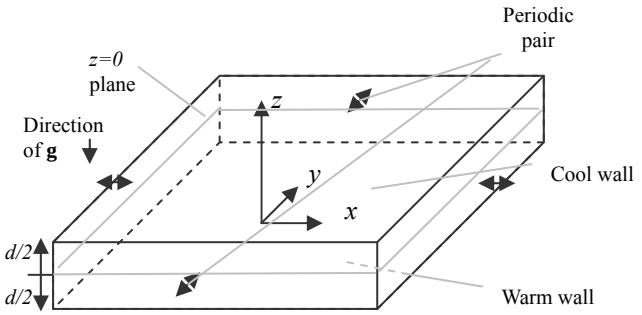

Figure 3 SIMULATION DOMAIN FOR RAYLEIGH-BENARD INSTABILITY

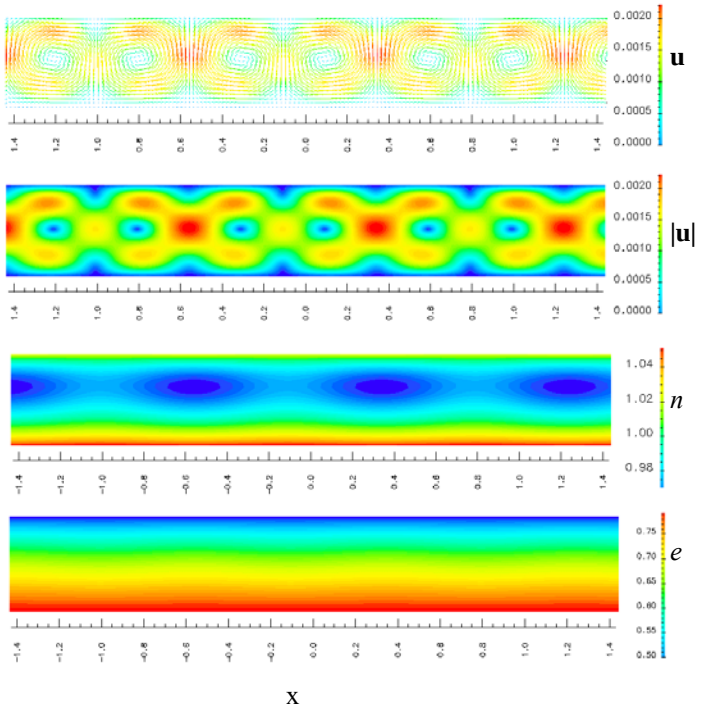

Figure 4. THE SIMULATION OF THE 2-D RAYLEIGH-BENARD INSTABILITY WITH CONVECTIVE ROLLS

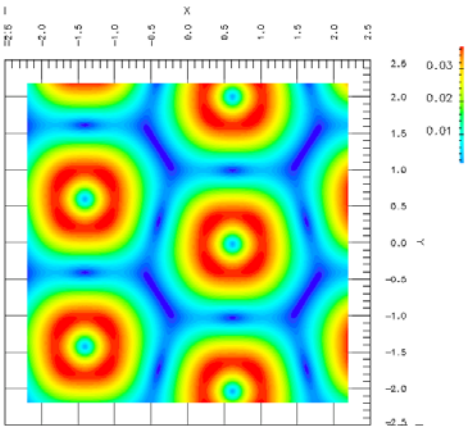

(1) |**u**| at z=d/2

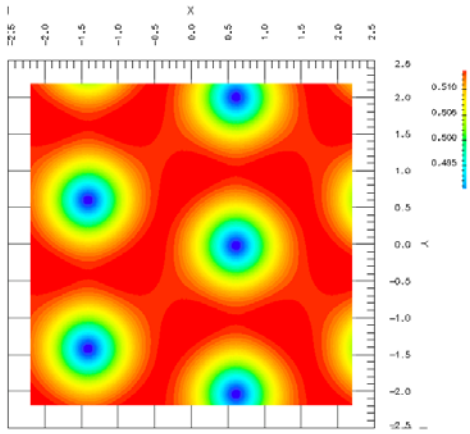

(2) *e* at z=d/2

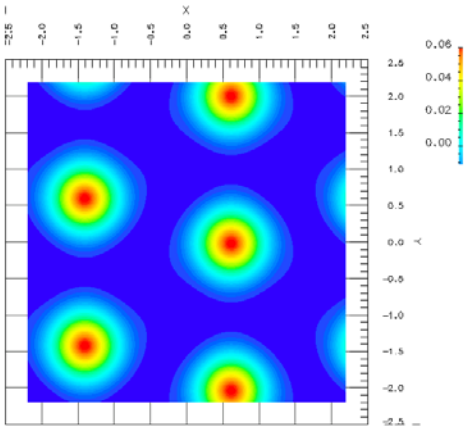

(3) *w* component at z=0

Figure 5. THE SIMULATION OF A 3D RAYLEIGH-BENARD CELL. FOR Ra=4000, THE CONVECTION SHOWS HEXAGONAL CELLULAR PATTERNS

The flows for 3-D RBC were calculated using an 8-core parallel computation code. The computation domain varies from 103x103x23 (for hexagonal cell case) to 123x123x23 (for convective rolls case). Similar parameter setting is employed for the 2D RBC case, but the *Ra* is increased to 4000. Some parameters are changed, including the Δx which is 0.04 in the present DLBM simulation, the gravitational pull is also doubled to 0.02. The top boundary uses a slip flow boundary, and the temperature is kept at a mean value using simple temperature relaxation to the mean value across time. The field is allowed to evolve for 10^5 time steps when the resultant flow is still evolving very slowly, with mean velocity magnitude change less then 10^{-4} of the typical value. Figure 5 shows the macroscopic flow field distributions of the velocity amplitude |**u**| at the top plate, the energy *e* at the top plate and the vertical velocity component *w* at the mid-plane. Hexagonal cells pattern are seen at Rayleigh number of around *Ra*=4000. For lower *Ra* values, convective rolls similar to the case of 2D-RBC are seen, but with a different wave number for the rolls. It is interesting to note that inside the hexagonal cells there exist very slow circular streaming flows other than the up-down circular motions. Fluid particles circulate around the centers of the hexagons in the RBC.

CONCLUSIONS

The dynamic lattice Boltzmann method (DLBM) is proposed and implemented. The DLBM code is validated and demonstrated for thermal fluid flow problems, such as the cavity flows and the 2D and 3D RBC flows. The locations of the viscous vortices in cavity flows and the onset of instability in RBC have been tested accordingly. They are in excellent agreement with classic literatures. With minimal efforts on modeling, macroscopic stress, flow fields, and thermal fluid properties all evolve naturally to attend flow patterns in good agreements to experimental results from literatures. The DLBM is a promising method in removing the incompressible and isothermal restrictions encountered by the conventional LBM. The homogenous and isotropic requirements are automatically satisfied by the DLBM to maintain the genuine features of the Boltzmann equation; hence the DLBM can then naturally predict thermal gas flows. The DLBM has removed the incompressible and thermal limitations encountered by conventional LBM. The simulation results based on DLBM exhibit indeed the physics of the original Boltzmann equation.

NOMENCLATURE

f	Velocity distribution function
f^{eq}	Maxwellian equilibrium distribution
f^*	Normalized velocity distribution function f / n_0
$\mathbf{C}^*$	Normalized peculiar velocity $(\mathbf{c}-\mathbf{u})/\sqrt{2RT}$
$\mathbf{r}^*, t^*$	Normalized space and time coordinates
$\mathbf{F}^*$	Normalized long range force $\mathbf{F}\tau_0 / a$
Ω^*	Normalized collision term $\Omega\tau_0 / n_0$
τ	Collision relaxation time
n^*	Normalized number density n / n_0
$\mathbf{u}^*$	Normalized macroscopic velocity $\mathbf{u} / a$
a	Most probable speed $\sqrt{2RT}$
n_0	Constant reference number density
τ_0	Constant reference time scale
a_0	Constant reference velocity scale
T_0	Constant reference temperature scale
Re	Reynolds number UH / ν
Ra	Rayleigh number $g\beta\Delta TH^3 / (\nu\alpha)$

ACKNOWLEDGMENTS

This work is supported by the ITC of Hong Kong Government through ITF under the Contract No.: GHP/028/08SZ.

REFERENCES

1. G.R. McNamara and G. Zanetti, (1988), "Use of the Boltzmann equation to simulate lattice-gas automata", *Physical Review Letters*. 61(20): p. 2332-2335.
2. S. Succi, (2001), *The Lattice Boltzmann Equation for Fluid Dynamics and Beyond*. Oxford: Clarendon Press.
3. D.A. Wolf-Gladrow, (2000), *Lattice Gas Cellular Automata and Lattice Boltzmann Models*. New York: Springer-Verlag.
4. S. Succi, A.A. Mohammad, and J. Horbach, (2007), "Lattice-Boltzmann simulation of dense nanoflows: a comparison with molecular dynamics and Navier-Stokes solutions", *International Journal of Modern Physics C*. 18(4): p. 667-675.
5. A. Masselot and B. Chopard, (1998), "A Lattice Boltzmann Model for Particle Transport and Deposition", *Europhysics Letters*. 42: p. 259-264.
6. L.-S. Luo, (1998), "Unified Theory of Lattice Boltzmann Models for Nonideal Gases", *Physical Review Letters*. 81(8): p. 1618-1621.
7. L.-S. Luo, (2000), "Theory of the Lattice Boltzmann Method: Lattice Boltzmann Models for Nonideal Gases", *Physical Review E*. 62(4): p. 4982-4996.
8. L.-S. Luo, (2000), "Some Recent Results on Discrete Velocity Models and Ramifications for Lattice Boltzmann Equation", *Computer Physics Communications*. 129: p. 63-74.
9. R. Benzi, S. Succi, and M. Vergassola, (1992), "The lattice Boltzmann equation: Theory and applications", *Physics Report*. 222(3): p. 145-197.
10. P. Lallemand and L.S. Luo, (2003), "Theory of the Lattice Boltzmann Method: Acoustic and Thermal Properties in Two and Three Dimensions", *Physical Review E*. 68(3): p. 3670601-3670625.
11. G. Karniadakis, A. Beskok, and N. Aluru, (2007), *Microflows and Nanoflows : Fundamentals and Simulation*. New York: Springer.
12. C.T. Hsu, S.W. Chiang, and K.F. Sin, (2010), "A Novel Dynamics Scheme for Solving Boltzmann Equation with Discrete Ordinate and Lattice Boltzmann Methods", *The 8th Asian Computational Fluid Dynamics Conference*. (Selected to submit to *Communications in Computational Physics*)
13. S.W. Chiang, K.F. Sin, and C.T. Hsu, (2010), "Numerical Simulation of Rayleigh-Benard Instability using Dynamic Lattice Boltzmann Method", *The 8th Asian Computational Fluid Dynamics Conference*.
14. B.J. Albright, et al., (2002), "Quiet direct simulation of Eulerian Fluid", *Physical Review E*. 65: p. 055302.
15. M.R. Smith, et al., (2009), "An improved Quiet Direct Simulation method for Eulerian fluids using a second-order scheme", *Journal of Computational Physics*. 228: p. 2213-2224.
16. C.T. Hsu, K.F. Sin, and S.W. Chiang, (2010), "Hybrid Parallelism for Boltzmann Equation Simulation with Dynamic Discrete Ordinate Method (DDOM)", *22nd International Conference on Parallel Computational Fluid Dynamics*. 17-22 May, Kaohsiung, Taiwan.
17. S. Chapman and T.G. Cowling, (1970), *The Mathematical Theory of Non-Uniform Gases*. 3rd ed. Cambridge: Cambridge University Press.
18. C.T. Hsu, S.W. Chiang, and K.F. Sin, (2010), "Dynamic Lattice Boltzmann Method for the Simulation of Cavity Flows with High Performance Computing", *22nd International Conference on Parallel Computational Fluid Dynamics*. 17-22 May, Kaohsiung, Taiwan.

19. D. Yu, R. Mei, and W. Shyy, (2002), "A multi-block lattice Boltzmann method for viscous fluid flows", *International Journal for Numerical Methods in Fluids*. 39: p. 99-120.
20. S. Hou, et al., (1995), "Simulation of Cavity Flow by the Lattice Boltzmann Method", *Journal of Computational Physics*. 118: p. 329-347.
21. W. Decker, W. Pesch, and A. Weber, (1994), "Spiral defect chaos in Rayleigh-Bénard convection", *Physical Review Letters*. 73(5): p. 648.
22. K. Krishan, et al., (2007), "Homology and symmetry breaking in Rayleigh-Bénard convection: Experiments and simulations", *Physics of Fluids*. 19(11): p. 117105.
23. W. Pesch, (1996), "Complex spatiotemporal convection patterns", *Chaos*. 6: p. 348.
24. M. Assenheimer and V. Steinberg, (1996), "Observation of Coexisting Upflow and Downflow Hexagons in Boussinesq Rayleigh-Bénard Convection", *Physical Review Letters*. 76(5): p. 756.
25. M. Assenheimer and V. Steinberg, (1993), "Rayleigh-Benard convection near the gas-liquid critical point", *Physical Review A*. 70(25): p. 3888.
26. P.G. Drazin, (2002), *Introduction to Hydrodynamic Stability*. Cambridge: Cambridge University Press.